Chinese Chemical Letters 35 (2024) 108287

Contents lists available at ScienceDirect

Chinese Chemical Letters

journal homepage: www.elsevier.com/locate/cclet

Alkyl-thiophene-alkyl linkers to construct double-cable conjugated polymers for single-component organic solar cells

Wenbin Lai[a,d,1], Safakath Karuthedath[c,e,1], Chengyi Xiao[b,*], Lei Meng[a,d], Frédéric Laquai[c], Weiwei Li[b,*], Yongfang Li[a,d]

[a] Beijing National Laboratory for Molecular Sciences, Key Laboratory of Organic Solids, Institute of Chemistry, Chinese Academy of Sciences, Beijing 100190, China
[b] Beijing Advanced Innovation Center for Soft Matter Science and Engineering & State Key Laboratory of Organic-Inorganic Composites, Beijing University of Chemical Technology, Beijing 100029, China
[c] King Abdullah University of Science and Technology (KAUST), KAUST Solar Center (KSC), Physical Sciences and Engineering Division (PSE), Material Science and Engineering Program (MSE), Thuwal 23955-6900, Kingdom of Saudi Arabia
[d] University of Chinese Academy of Sciences, Beijing 100049, China
[e] Institute of Materials Research, Tsinghua Shenzhen International Graduate School, Tsinghua University, Shenzhen 518055, China

ARTICLE INFO

Article history:
Received 17 January 2023
Revised 8 February 2023
Accepted 1 March 2023
Available online 5 March 2023

Keywords:
Double-cable conjugated polymer
Single-component organic solar cell
Crystallinity
Semirigid linkers
Alkyl-thiophene-alkyl

ABSTRACT

In this work, semirigid linkers of the alkyl-thiophene-alkyl structure are developed to construct double-cable polymers. Three alkyl units, propyl (C_3H_6), hexyl (C_6H_{12}), and dodecyl ($C_{12}H_{24}$), are applied as semirigid linkers, yielding three double-cable polymers: PBC6-T, PBC12-T, and PBC24-T, respectively. PBC12-T which uses C_6H_{12}-thiophene-C_6H_{12} linkers is found to exhibit the best device efficiency of 5.56%, while PBC6-T and PBC24-T with shorter or longer linkers yield device efficiencies of only 2.65% and 1.09% in single-component organic solar cells (SCOSCs). Further studies reveal that PBC12-T exhibits higher crystallinity and improved charge transport, resulting in better efficiencies. Our work provides an approach to construct double-cable conjugated polymers with long alkyl linkers, and it shows the importance of the linker length for the photovoltaic performance of SCOSCs.

Recent development of non-fullerene acceptors with near-infrared absorptions has propelled power conversion efficiencies (PCEs) of organic solar cells (OSCs) to over 19% [1–8]. However, in the laboratory to commercial product translation, one needs to consider the "golden triangle": A combination of low cost, high PCEs, and long-term stability [9,10]. In particular, the long-term stability of bulk-heterojunction (BHJ) OSCs has impeded their wide-scale commercialization [11,12]. As an alternative, double-cable conjugated polymers, with covalently-linked donor and acceptor segments, have been used in single-component OSCs (SCOSCs), exhibiting improved shelf, photo and thermal stability [13–17]. Furthermore, SCOSCs offer less processing complexity, which effectively lowers the cost of the photoactive layers and fabrication processes [18–23]. However, the PCEs of double-cable conjugated polymer-based SCOSCs are still lacking behind the BHJ-OSCs due to limited materials and the difficulty to tune the nanoscale donor–acceptor separation in thin films [16].

In the search for high-performance SCOSC materials, block polymers, molecular dyads, and double-cable polymers have been developed, of which double-cable polymers contain conjugated polymers as the electron-donating backbone and aromatic side units as acceptors [15-17,24,25]. For example, the incorporation of near-infrared non-fullerene acceptors as side units into double-cable polymers with an asymmetric structure has promoted the PCEs of SCOSCs to more than 10% due to enhanced photo-current generation [15]. Meanwhile, various strategies have been used to obtain well-ordered nanoscale phase separation for double-cable conjugated polymers, including rational material design (such as symmetric or asymmetric structures) and post-processing treatment [26–31]. For instance, the miscibility between the conjugated backbone and pendant acceptors can provide a large donor/acceptor interface area, particularly in the amorphous regions, which is beneficial for exciton dissociation and improves the fill factor (FF) of SCOSCs. This miscibility control has promoted the PCE to 8.4% with FF values approaching 0.7 in SCOSCs [24,32]. In addition to the conjugated donor and acceptor units, the linkers, which determine the degree of freedom of conjugated backbones and side units, are equally important, since they modulate molecular orientation

* Corresponding authors.
E-mail addresses: xiaocy@mail.buct.edu.cn (C. Xiao), liweiwei@iccas.ac.cn (W. Li).
[1] These authors contributed equally to this work.

https://doi.org/10.1016/j.cclet.2023.108287
1001-8417/

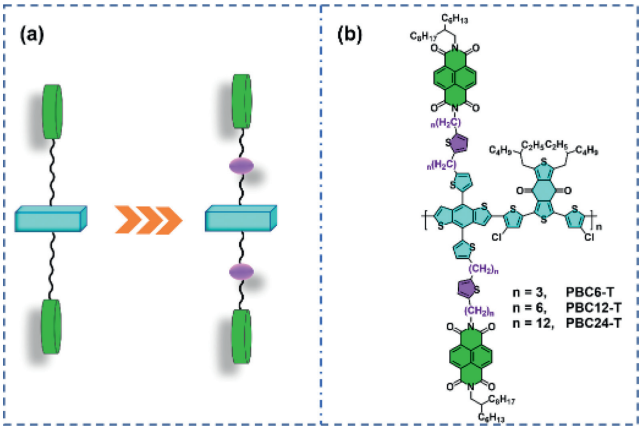

Scheme 1. (a) Schematic diagram and (b) chemical structures of double-cable conjugated polymers with semirigid linkers in this work.

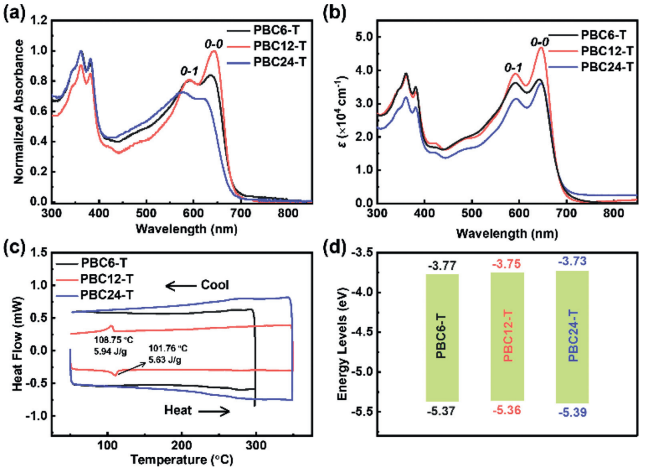

Fig. 1. The optical absorption spectra of PBC6-T, PBC12-T and PBC24-T in (a) chloroform solution and (b) thin films (with absorption coefficients). (c) The DSC heating and cooling traces (second cycle) and (d) the energy levels of the polymer PBC6-T, PBC12-T and PBC24-T.

and nano-scale phase separation. Our previous works have demonstrated that the length of the alkyl linkers can significantly change the morphology of thin films and it can reduce non-radiative recombination of charge carriers in SCOSCs [33–35]. However, it remains challenging to obtain materials with very long alkyl linkers due to the intrinsic low solubility of alkyl molecules longer than $C_{20}H_{40}$ which usually are waxy oils or solids, and the highly challenging synthesis.

In this work, we have successfully incorporated semirigid linkers, specifically 2,5-disubstituted alkyl thiophene, into naphthalene diimides-based double-cable conjugated polymers (Scheme 1). This molecular design provided a route to realize long linkers with improved solubility in common organic solvents. Three different alkyl chains, ranging from propyl (C_3H_6) over hexyl (C_6H_{12}) to dodecyl ($C_{12}H_{24}$), were introduced into 2,5-disubstituted thiophenes. Further material characterizations show that the length of the semirigid linker has a distinct impact on the aggregation and crystallinity of the polymer films. These differences resulted in different exciton dynamics and carrier recombination kinetics, as well as photovoltaic performance. Our results emphasize the importance of semirigid linkers in tuning the crystallinity and photophysical processes in SCOSCs.

The structures of the double-cable polymers with semirigid linkers developed in this work are shown in Scheme 1. The detailed synthesis procedures are summarized in Scheme S1 (Supporting information). The double-cable conjugated polymers were obtained through *Stille* coupling polymerization by using the "functionalization-polymerization" method according to previous reports [35–37]. These polymers are denoted as PBC6-T, PBC12-T and PBC24-T corresponding to propyl (C_3H_6), hexyl (C_6H_{12}), and dodecyl ($C_{12}H_{24}$) disubstituted thiophene linkers, respectively. All these polymers exhibited good solubility in chlorobenzene, *ortho*-dichlorobenzene (*o*-DCB), and toluene as solvents. Their molecular weights were measured by gel permeation chromatography (GPC) measurements with *o*-DCB as the eluent against polystyrene standards at 140 °C. As shown in Table 1, the number-average molecular weights (M_n) of PBC6-T, PBC12-T and PBC24-T are 62.2, 38.9 and 23.8 kg/mol, and the polydispersity indexes (PDIs) are 1.50, 2.12 and 1.66, respectively.

The absorption spectra of these double-cable conjugated polymers are shown in Figs. 1a and b, and optical properties are summarized in Table 1. The peaks at 300–400 nm can be attributed to the contribution of pendant naphthalene diimide (NDI) units, while the peaks in the range of 500–700 nm can be attributed to the conjugated backbone. Bathochromic shifts of ~50 nm are observed between solution and thin films in all polymers. The larger shifts observed for PBC12-T and PBC24-T indicate stronger aggregations in thin films. The higher *0-0* peaks than *0-1* peaks indicate a typical *J*-type aggregation [38]. PBC12-T exhibited larger *0-0*/*0-1* intensity ratios than those of PBC6-T and PBC24-T, suggesting enhanced aggregation of the conjugated backbones [15]. The excellent thermal stability of these polymers was demonstrated by thermal gravimetric analysis (TGA) measurements with only 5% weight loss at above 400 °C (Fig. S1 in Supporting information). Heating and cooling traces determined by differential scanning calorimetry (DSC) measurements are shown in Fig. 1c. PBC6-T and PBC24-T showed no phase transition peaks, while PBC12-T shows several transition peaks, indicating crystallization during the cooling cycle. As shown in Fig. 1d and Table 1, the cyclic voltammetry (CV) measurements (Fig. S2 in Supporting information) determined the similar highest occupied molecular orbital (HOMO) and lowest unoccupied molecular orbital (LUMO) energy levels of these polymers due to the identical donor and acceptor structures.

These double-cable conjugated polymers with semirigid linkers were then applied in SCOSCs using the inverted layout ITO/ZnO/active layers/MoO_3/Ag [15]. Representative *J*-*V* curves of devices are shown in Fig. 2a and the figures-of-merit are summarized in Table 2. After optimization of the processing conditions, including processing additives and post-processing thermal

Table 1
Molecular weight and optical properties of the polymers.

Polymer	M_n (kg/mol)	M_w (kg/mol)	PDI	$E_g^{sol,\ a}$ (eV)	$E_g^{film,\ a}$ (eV)	E_{HOMO}[b] (eV)	E_{LUMO}[c] (eV)
PBC6-T	62.2	93.0	1.50	1.81	1.77	−5.37	−3.77
PBC12-T	38.9	82.6	2.12	1.82	1.77	−5.36	−3.75
PBC24-T	23.8	39.5	1.66	1.85	1.77	−5.39	−3.73

[a] Optical bandgap was calculated through the onset of the absorption edge.
[b] Calculated by $E_{HOMO} = -4.80\ eV - E_{ox}$.
[c] $E_{LUMO} = -E_{red} - 4.80\ eV$.

Table 2
Photovoltaic performances of these polymers. Charge carrier mobilities determined by SCLC measurement.

Polymers	V_{OC}[a] (V)	J_{SC}[a] (mA/cm^2)	*FF*[a]	PCE[a] (%)	μ_h[b] (cm^2 V^{-1} s^{-1})
PBC6-T	0.92 (0.91±0.016)	7.73 (7.44±0.28)	0.37 (0.37±0.018)	2.65 (2.47±0.19)	2.3×10^{-3}
PBC12-T	0.93 (0.93±0.005)	9.78 (9.64±0.15)	0.61 (0.60±0.005)	5.56 (5.45±0.09)	5.1×10^{-3}
PBC24-T	0.91 (0.90±0.027)	3.50 (3.45±0.07)	0.34 (0.33±0.014)	1.09 (1.02±0.05)	6.4×10^{-5}

[a] The average parameters are obtained from 6 parallel devices.
[b] Hole mobility extracted from transfer curves obtained from OFET devices.

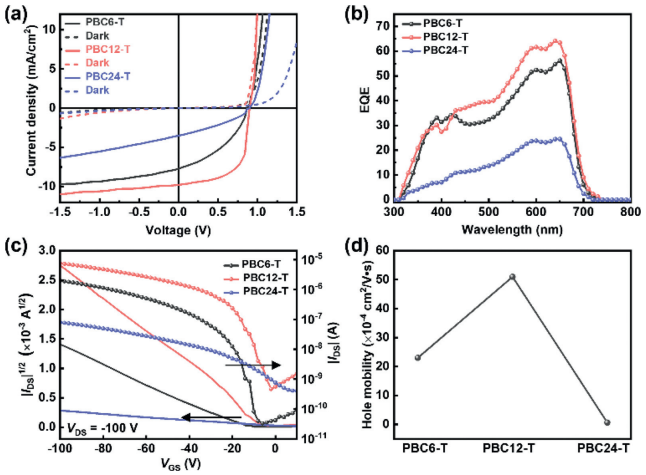

Fig. 2. (a) *J-V* characteristics and (b) the corresponding EQE spectra of SCOSCs based on PBC6-T, PBC12-T and PBC24-T. (c) Typical p-type transfer curves of representative OFET devices of these polymers. (d) The μ_hs of these polymers calculated from the OFET measurements.

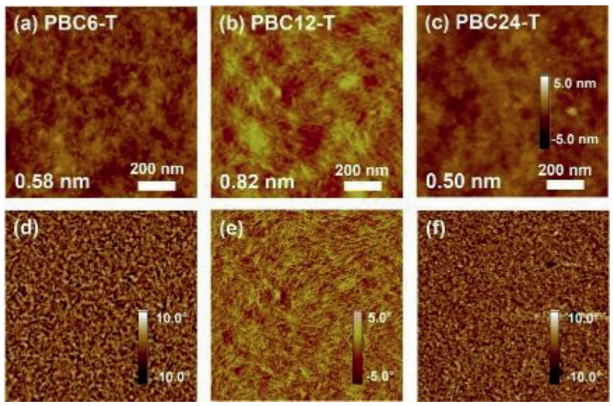

Fig. 3. The tapping mode AFM (a-c) height and (d-f) phase images (3 × 3 μm) of these polymer films.

annealing, the highest performance SCOSCs were obtained from toluene solution with 0.5 vol% 1,8-diiodooctane (DIO) as an additive and thermal annealing at 150 °C for 10 min (Tables S1-S6 in Supporting information). As shown in Fig. 2a and Table 2, all the SCOSCs exhibited similar V_{OC}s (open-circuit voltages) of 0.91–0.93 V due to the similar frontier orbital energy levels. Compared with PBC6-T and PBC24-T, PBC12-T-based SCOSCs exhibited a higher J_{SC} (short-circuit current density) of 9.78 mA/cm^2 and FF of 0.61, resulting in a PCE of 5.56%. The enhanced J_{SC} in PBC12-T-based SCOSCs is also reflected in their high EQE (external quantum efficiency) spectra approaching 60%, as shown in Fig. 2b. Moreover, although the PBC24-T-based devices showed similar FF values compared to PBC6-T, the lower J_{SC} limited the PCE to only 1.09%. Next, we fabricated organic field-effect transistors (OFETs) on a commercial Si/SiO_2 substrate using the bottom-gate bottom contact device structure and an octadecyltrichlorosilane (OTS) monolayer [39,40]. All the polymers exhibited p-type characteristics, while the electron mobility was too low to be measured. As shown in Fig. 2c, the calculated hole mobilities (μ_h) are plotted in Fig. 2d and summarized also in Table 2. The OFET based on PBC6-T showed a relatively high μ_h of 2.3×10^{-3} cm^2 V^{-1} s^{-1}, which was enhanced to 5.1×10^{-3} cm^2 V^{-1} s^{-1} for PBC12-T based devices and decreased to 6.4×10^{-5} cm^2 V^{-1} s^{-1} for PBC24-T, respectively. The hole mobilities in the SCLC measurement showed a similar trend to those in the OFETs measurement as shown in Fig. S3 (Supporting information). The different charge carrier mobilities are partially responsible for the different J_{SC}s in SCOSCs. The significantly lower hole mobility of PBC24-T is surprising and requires further investigation. In fact, the very long linkers influence the backbone packing of PBC12-T [34], which could be confirmed in this work, but the precise relation between the morphology and charge carrier mobility remains unclear and requires further studies.

The thin film morphology of the polymers was characterized by atomic force microscopy (AFM) measurement. As shown in Fig. 3, all these polymers exhibited "fiber-like" microstructures in both the height and phase images. However, the fibers in PBC6-T and PBC24-T films were significantly smaller with low root-mean-square (RMS) roughness of 0.58 nm and 0.50 nm (Figs. 3a and c), respectively. Due to the better crystallinity of PBC12-T, the corresponding films showed larger microfibers in films with a higher RMS value of 0.82 nm as shown in Fig. 3b. The larger "fiber-like" grains and better nano-scale phase separation of PBC12-T facilitate exciton-to-charge conversion and charge carrier transport, enhancing its PCE in SCOSCs [37].

Next, we employed two-dimensional grazing-incidence X-ray scattering with wide-angle (GIWAXS) and medium-angle (GIMAXS) to investigate the molecular packing of the polymers. The GIWAXS profiles are shown in Figs. 4a-c and the crystallographic parameters are summarized in Table S8 (Supporting information). From the GIWAXS patterns in Figs. 4a-c, it appears that all three polymers preferentially show a "face-on" orientation [41,42] with in-plane (IP) lamellar (*h*00) peaks and out-of-plane (OOP) π-π stacking (010) peak. The intensities of all these peaks were significantly enhanced after thermally annealing at 150 °C (Fig. S3 in Supporting information and Figs. 4a-c, Fig. S4 in Supporting information and Figs. 4d-f). According to the GIMAXS images in Figs. 4d-f, all polymers exhibited multiple scattering peaks in the IP direction, which have been assigned to the (100) to (300) lattice planes as shown in Figs. 4g-i. Clearly, as shown in Table S8, the calculated lamellar *d*-spacing in the alkyl chain direction increased significantly from 37.0 Å for PBC6-T to 45.5 Å for PBC12-T and to 58.2 Å for PBC24-T, respectively, as a consequence of the increased linker lengths and indicates no ordering transition, which is also consistent with the NDI-based double-cable conjugated polymers [34,35]. The PBC12-T-based films exhibited the largest coherence length (*CL*) value of 10.5 nm compared to PBC6-T (5.84 nm) and PBC24-T (3.16 nm) due to the improved crystallinity of PBC12-T as indicated by the DSC measurements. For the OOP direction, all three polymers showed similar π-π stacking with similar $d_{(010)}$ values of 3.66–3.68 nm

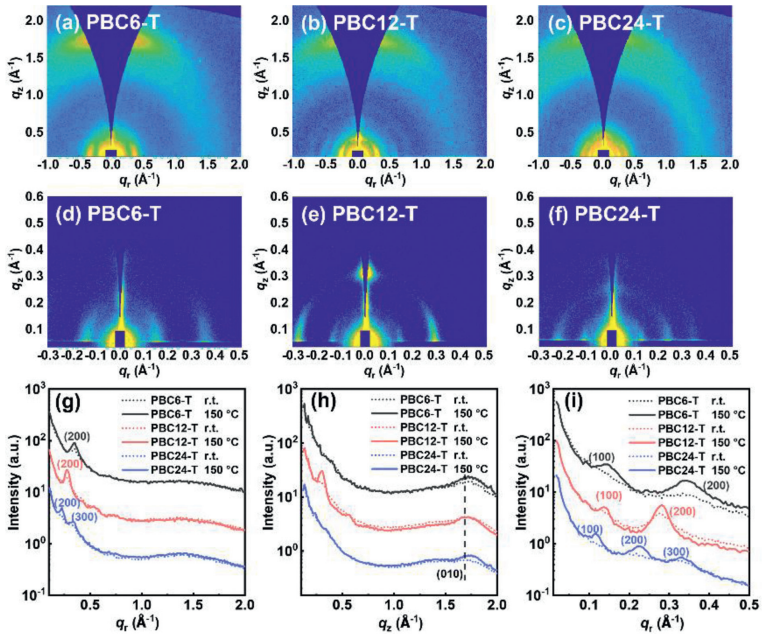

Fig. 4. (a-c) GIWAXS and (d-f) GIMAXS profiles on the Si substrates of PBC6-T, PBC12-T and PBC24-T thin films. (g) In-plane and (h) out-of-plane plots of the corresponding GIWAXS images. (i) In-plane cutlines of the GIMAXS images.

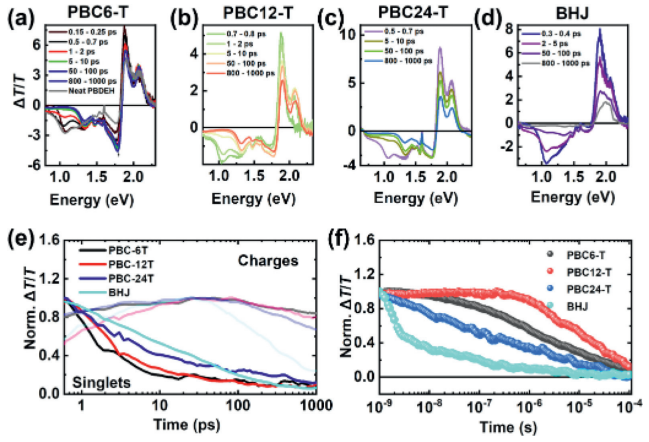

Fig. 5. The ps-ns TA spectra of (a) PBC6-T, (b) PBC12-T, (c) PBC24-T and (d) BHJ films after exciting at 650 nm. (e) ps-ns TA kinetics of charge-dominated (1.65–1.75 eV) and singlet-dominated (0.9–1 eV) spectral regions. (f) ns-μs TA kinetics of 1.65–1.75 eV band after exciting at 532 nm.

and corresponding *CL* values of 1.20–2.35 nm. Hence, we conclude that the increased linkers increase the degree of freedom of the covalent-linked donor backbone and NDI acceptors, which helps the packing of the polymers in thin films. However, excessively long linkers corrupt the interaction between the donor and acceptor parts, and the high crystallinity of NDI hampers the crystallization of the polymer donor backbone [30].

Next, we performed ultrafast transient absorption (TA) spectroscopy on thin films to unravel the photo-excited state dynamics. Figs. 5a-d show the picosecond to nanosecond (ps-ns) TA spectra of thin films after excitation at 650 nm. The positive $\Delta T/T$ signal represents the material's ground state bleach (PB), and the negative $\Delta T/T$ is caused by photo-induced absorption (PA) of excited states [43]. Fig. 5a shows the ps-ns TA spectra of a PBC6-T film. We assigned the PA band at ~1.02 eV to singlet state-induced absorption of PBEH as it matches with the neat TA spectra of neat PBEH films (Fig. S5 in Supporting information). We note that the PA band at 1.02 eV decayed faster than the bands at 1.3–1.34 eV and 1.65–1.75 eV. This implies that the bands originate from different species, namely singlet states and charge carriers. Notably, the ps-ns TA spectra of both PBC12-T and PBC24-T showed a similar spectral evolution (Figs. 5b and c). However, we note that the ps-ns TA spectra of BHJ films point to very limited charge generation, in line with the poor PCE of the devices based on BHJ-type films (Fig. 5d). Fig. 5e shows the kinetics of selected spectral regions (0.9–1.0 eV for singlet states and 1.65–1.75 eV for charges). However, in all samples, the charge generation is concluded within ~20–30 ps. We note that, though the PCE is low, the BHJ film showed some charge generation in the first 20–30 ps, while most of the singlet excited states decayed back to the ground state without undergoing charge transfer.

Having discussed the impact of linker length on charge generation, we now discuss charge carrier recombination. The BHJ film showed fast charge carrier recombination, suggesting that BHJ devices are not only limited by inefficient charge generation, but also by fast charge carrier recombination. This points to the importance of using linkers that enhance the charge carrier generation and simultaneously reduce the charge carrier recombination. The charge carriers in PBC6-T and PBC12-T thin films showed similar charge carrier decay dynamics, while PBC24-T exhibited significantly faster charge carrier decay. Since the ps-ns TA cannot probe the entire charge recombination process, we conducted ns-μs TA experiments to monitor the entire charge carrier recombination dynamics to understand its impact on device performance. On the ns-μs time scale, singlet excited states are no longer observed and charge carriers dominate the TA spectra and dynamics. Fig. 5f shows the ns-μs charge carrier decay dynamics of all four films after excitation at 532 nm. The corresponding ns-μs TA spectra are provided in Fig. S6. Clearly, the decay of the charge-induced absorption is slower for PB12-T than for PBC6-T. The charge carrier decay is even faster in PBC24-T and BHJ films.

In conclusion, we introduced three linkers with different lengths (C_6H_{12}, $C_{12}H_{24}$ and $C_{24}H_{48}$) using alkyl-thiophene-alkyl linkers into double-cable polymers. PBC12-T with intermediate linker length exhibited enhanced crystallinity due to the increased degree of freedom provided by the linker, which was found to

be beneficial for charge transport in SCOSCs. The best compromise of charge carrier generation and recombination kinetics provided PCEs of 5.56% for PBC12-T-based SCOSCs, while PBC6-T with shorter linkers and PBC24-T with longer linkers showed lower efficiencies. Our results provide guidance on the design of linkers in double-cable conjugated polymers and emphasize the importance of linker length in controlling intermolecular packing, photophysical processes, and photon-to-electron conversion yields.

Declaration of competing interest

The authors declare that they have no known competing financial interests or personal relationships that could have appeared to influence the work reported in this paper.

Acknowledgments

This study is jointly supported by the Beijing Natural Science Foundation (No. JQ21006), the Ministry of Science and Technology (No. 2018YFA0208504), and the National Natural Science Foundation (Nos. 92163128, 52073016, 21905018) of China. This work was further supported by the Fundamental Research Funds for the Central Universities (Nos. buctrc201828, XK1802-2), Open Project of State Key Laboratory of Organic-Inorganic Composites (No. oic-202201006), and Open Project of State Key Laboratory of Supramolecular Structure and Materials (No. sklssm202209). The research reported in this publication was supported by funding from the King Abdullah University of Science and Technology (KAUST).

References

[1] Y. Lin, J. Wang, Z.G. Zhang, et al., Adv. Mater. 27 (2015) 1170–1174.
[2] J. Yuan, Y. Zhang, L. Zhou, et al., Joule 3 (2019) 1140–1151.
[3] S. Chen, D. Meng, J. Huang, et al., CCS Chem. 3 (2021) 78–84.
[4] L. Zhu, M. Zhang, J. Xu, et al., Nat. Mater. 21 (2022) 656–663.
[5] Y. Cui, Y. Xu, H. Yao, et al., Adv. Mater. 33 (2021) e2102420.
[6] L. Zhan, S. Li, Y. Li, et al., Joule 6 (2022) 662–675.
[7] X. Kong, J. Zhang, L. Meng, et al., CCS Chem. (2022) 1–10.
[8] Y.H. Liu, B.W. Liu, C.Q. Ma, et al., Sci. China Chem. 65 (2022) 1457–1497.
[9] S. Park, T. Kim, S. Yoon, et al., Adv. Mater. 32 (2020) e2002217.
[10] L. Meng, J. You, Y. Yang, Nat. Commun. 9 (2018) 5265.
[11] P. Cheng, X.W. Zhan, Chem. Soc. Rev. 45 (2016) 2544–2582.
[12] B. Walker, A.B. Tamayo, X.D. Dang, et al., Adv. Funct. Mater. 19 (2009) 3063–3069.
[13] Y. He, N. Li, T. Heumüller, et al., Joule 6 (2022) 1160–1171.
[14] Y.K. He, T. Heumuller, W.B. Lai, et al., Adv. Energy Mater. 9 (2019) 1900409.
[15] S. Liang, B. Liu, S. Karuthedath, et al., Angew. Chem. Int. Ed. 61 (2022) e202209316.
[16] S. Liang, X. Jiang, C. Xiao, et al., Acc. Chem. Res. 54 (2021) 2227–2237.
[17] J. Roncali, I. Grosu, Adv. Sci. 6 (2019) 1801026.
[18] J. Roncali, Adv. Energy Mater. 1 (2011) 147–160.
[19] D.D. Xia, C. Li, W.W. Li, Chem. Rec. 19 (2019) 962–972.
[20] Y. Liu, B. Liu, C.Q. Ma, et al., Sci. China Chem. 65 (2021) 224–268.
[21] C.H. Liu, C.Y. Xiao, C.C. Xie, W.W. Li, Nano Energy 89 (2021) 106399.
[22] C. Xie, X. Jiang, Q. Zhu, et al., Small Methods 5 (2021) e2100481.
[23] C. Xie, C. Xiao, X. Jiang, et al., Macromolecules 55 (2021) 322–330.
[24] Y. Wu, J. Guo, W. Wang, et al., Joule 5 (2021) 1800–1815.
[25] D. Wang, Z.F. Yang, F. Liu, et al., Chin. Chem. Lett. 33 (2022) 466–469.
[26] A.M. Ramos, M.T. Rispens, J.K.J. van Duren, et al., J. Am. Chem. Soc. 123 (2001) 6714–6715.
[27] F. Zhang, M. Svensson, M.R. Andersson, et al., Adv. Mater. 13 (2001) 1871–1874.
[28] Z.A. Tan, J. Hou, Y. He, et al., Macromolecules 40 (2007) 1868–1873.
[29] Y.H. Geng, Acta Phys. Chim. Sin. 35 (2019) 1311–1312.
[30] C. Li, X. Wu, X. Sui, et al., Angew. Chem. Int. Ed. 58 (2019) 15532–15540.
[31] J. Song, Z. Bo, Chin. Chem. Lett. 34 (2023) 108163.
[32] J. Guo, Y. Wu, W. Wang, et al., Sol. RRL 6 (2022) 2101024.
[33] J. Wang, X.D. Jiang, H.B. Wu, et al., Nat. Commun. 12 (2021) 6679.
[34] G. Feng, W. Tan, S. Karuthedath, et al., Angew. Chem. Int. Ed. 60 (2021) 25499–25507.
[35] Z.J. Hu, C.Y. Xiao, W.L. Tan, et al., Macromolecules 55 (2022) 5188–5196.
[36] G.T. Feng, J.Y. Li, Y.K. He, et al., Joule 3 (2019) 1765–1781.
[37] X. Jiang, J. Yang, S. Karuthedath, et al., Angew. Chem. Int. Ed. 59 (2020) 21683–21692.
[38] F.C. Spano, Acc. Chem. Res. 43 (2010) 429–439.
[39] C. Wang, H. Dong, W. Hu, et al., Chem. Rev. 112 (2012) 2208–2267.
[40] C.Y. Xiao, C. Li, F. Liu, et al., J. Mater. Chem. C 8 (2020) 5370–5374.
[41] H. Sirringhaus, P.J. Brown, R.H. Friend, et al., Nature 401 (1999) 685–688.
[42] C. Xiao, G. Zhao, A. Zhang, et al., Adv. Mater. 27 (2015) 4963–4968.
[43] S. Karuthedath, A. Melianas, Z. Kan, et al., J. Mater. Chem. A 6 (2018) 7428–7438.